Journal of Integrative Agriculture 2026, 25(8): 3153–3168

Available online at ScienceDirect

Journal of Integrative Agriculture



RESEARCH ARTICLE

Two genes of cytochrome P450 regulate plant height *via* brassinosteroid biosynthesis in *Brassica napus*

Qianqian Zheng[1*], Xinhua Wang[1*], Zhenzhen Wang[1], Yi Zhang[1], Hao Wang[3], Kangxi Du[3], Shaohong Fu[2], Wanzhuo Gong[2], Hua Yuan[3], Weilan Chen[3], Bin Tu[3], Jin Yang[2#], Yun Li[2#], Ting Li[1#]

[1] *State Key Laboratory of Crop Gene Exploration and Utilization in Southwest China/Sichuan Agricultural University, Chengdu 611130, China*
[2] *Chengdu Research Branch, Chengdu Academy of Agriculture and Forestry Sciences/National Rapeseed Genetic Improvement Center, Chengdu 611130, China*
[3] *Rice Research Institute, Sichuan Agricultural University, Chengdu 611130, China*

Highlights

- This study identified two cytochrome P450 genes, *BnaA10.CYP90A1* and *BnaC09.CYP90A1*, as key regulators of plant height in *Brassica napus*, highlighting their roles in brassinosteroid biosynthesis and plant growth modulation.
- Mutations in *BnaA10.CYP90A1* and *BnaC09.CYP90A1* genes lead to reduced levels of bioactive brassinosteroids, significantly impairing cell elongation and causing a dwarf phenotype in rapeseed.
- The single mutation of *BnaA10.CYP90A1* produced semi-dwarf plants, suggesting its potential for developing new rapeseed cultivars with optimized plant height for enhanced yield and mechanical harvesting efficiency.

Abstract

Rapeseed (*Brassica napus*) is one of the most important oil crops worldwide and provides a major source of edible vegetable oil. Currently, manipulating plant height with branching effectively balances biomass and yields. However, the genetic mechanisms to control plant height remain largely unknown in rapeseed. To address this gap, we isolated an extremely dwarf mutant (*dm1*) from ethyl-methanesulfonate (EMS) mutagenesis and revealed that the dwarfism results from a significant reduction in cell length. Bulk segregant analysis (BSA) identified *BnaA10.CYP90A1* and *BnaC09.CYP90A1* as the causative genes of *dm1*. Both genes encoded the proteins homologous to the *Arabidopsis* cytochrome P450 AtCPD/AtCYP90A1, which is crucial for brassinosteroid (BR) biosynthesis. In this regard, we demonstrated reduced levels of bioactive BRs, castasterone (CS), and its precursor 6-deoxoCS in *dm1*, resulting in down-regulation of various genes involved in cell expansion. The reduced BR levels also caused negative feedback, promoting the expression of BR biosynthetic genes in *dm1*. Furthermore, we proved that the single mutation of *BnaA10.CYP90A1* gene conferred semi-dwarfism, potentially beneficial for producing an ideal type of plant to improve cultivars with a balance of yield and machinery harvest through genetic modifications. Collectively, these findings highlighted the critical role of BnaCYP90A1s in BR biosynthesis and validated their influence on plant height regulation in rapeseed.

Keywords: plant height, BR biosynthesis, cytochrome P450, *Brassica napus*

1. Introduction

Brassica napus L. (rapeseed) is one of the most important oil crops worldwide. Recently, hybrid breeding in rapeseed has been rapidly developed to meet the growing demand for vegetable oils (Hu *et al.* 2017). However, most hybrids are 2 m or taller, making them prone to lodging and increasing the difficulty of mechanical harvesting. As a result, an ideal plant type has been proposed, a semi-dwarf plant with lobed leaves and compact architecture (Zheng *et al.* 2022). This type is beneficial for increasing yield through higher

Received 9 August 2024; Received in revised form 31 October 2024; Accepted 21 November 2024; Available online 12 December 2024
[#]Correspondence Ting Li, Tel: +86-28-86293167, E-mail: tinli@sicau.edu.cn; Yun Li, Tel: +86-28-82746572, E-mail: liyunxpzh@163.com; Jin Yang, Tel: +86-28-82746572, E-mail: yjjing@163.com
[*] These authors contributed equally to this study.

© 2026 CAAS. Publishing services by Elsevier B.V. on behalf of KeAi Communications Co. Ltd. This is an open access article under the CC BY-NC-ND license (http://creativecommons.org/licenses/by-nc-nd/4.0/). Peer review under responsibility of Editorial Board of *Journal of Integrative Agriculture*.
doi: 10.1016/j.jia.2024.12.016

planting density and reducing production cost by facilitating mechanized harvesting (Hu *et al.* 2017; Liu *et al.* 2022).

Identification of semi-dwarf genes is crucial for improving plant architecture and yield performance in rapeseed (Hu *et al.* 2021). For this purpose, many studies have used forward screening and fine-mapping strategies. Genes *DS-1* and *DS-3* that encode DELLA proteins were identified in the semi-dwarf plants *ds1* and *ds3* (Liu *et al.* 2010; Zhao *et al.* 2017). They serve as core repressors of the transduction of gibberellic acid signal and orchestrate plant stem growth by inhibiting cell division and elongation (Achard *et al.* 2009; Du *et al.* 2015). Similarly, *NDOLE-3-ACETIC ACID 7* (*BnaC05.IAA7*, *BnaA03.IAA7*) and *BnaA03.IAA13* function as negative regulators in auxin signal to reduce plant height by restricting internode growth (Cheng *et al.* 2019; Li *et al.* 2019; Ping *et al.* 2022; Gao *et al.* 2024). Alternatively, in a reverse genetic study, knocking out *MORE AXILLARY GROWTH 1* (*BnaMAX1*) results in a semi-dwarf and branch-increased phenotype in rapeseed, because it affects the biosynthesis of strigolactones (Zheng *et al.* 2020).

In addition, brassinosteroids (BRs) are a class of steroidal phytohormones, pivotal for regulating plant height (Kim and Russinova 2020; Song *et al.* 2023). Plants with reduced intrinsic levels of BR or attenuated sensitivity to BR are generally dwarfed, whereas exogenous application of brassinolide (BL), a bioactive form of BR, promotes stem elongation (Gudesblat and Russinova 2011; Zhang *et al.* 2022; Chen *et al.* 2024). Additionally, *BRASSINOSTEROID INSENSITIVE 1* (*BnaBRI1*), *DWARF 4* (*BnaDF4*), and *BRASSINOSTEROID-INSENSITIVE 2* (*BnaBIN2*) are core regulators of BR signaling that affect cell elongation in rapeseed stems (Song *et al.* 2022; Zhao *et al.* 2022; Li *et al.* 2023). These studies suggest that both BR biosynthesis and signal transduction are crucial for regulating plant growth.

However, it remains unknown whether key components of the BR biosynthetic pathway regulate plant height in rapeseed. BR biosynthesis in plants involves multiple interconnected pathways, beginning with the conversion of campesterol (CR) into campestanol (CN) or 6-deoxocathasterone (6-deoxoCT) through early or late C22 oxidation pathways, followed by the conversion of CN into BL *via* early or late C6 oxidation pathways (Zhao and Li 2012; Zebosi *et al.* 2024). Among these pathways, the early C22 oxidation and late C6 oxidation pathways are the predominant routes in cruciferous plants (Wei and Li 2020).

In the predominant BR biosynthetic pathways, CR, a BR-specific biosynthetic precursor, undergoes successive catalysis for forming 6-deoxoCT by cytochrome P450 enzymes (CYP450), including DWARF4/CYP90B1, CONSTITUTIVE PHOTOMORPHOGENESIS AND DWARFISM (CPD/CYP90A1), and steroid 5α-reductase DE-ETIOLATED 2 (DET2) (Noguchi *et al.* 1999; Bancoş *et al.* 2002; Bancos *et al.* 2006; Kim *et al.* 2006). In the next step, 6-deoxoCT is catalyzed by ROTUNDIFOLIA 3 (ROT3/CYP90D1), DWARF 2 (D2/CYP90D2), and D11/CYP724B1 to form 6-deoxotyphasterol (6-deoxoTY) (Kim *et al.* 1998; Hong *et al.* 2005; Wan *et al.* 2009). Finally, 6-deoxoTY is converted into typhasterol (TY) and castasterone (CS) to form BL. Both CS and BL are bioactive BRs in rapeseed (Kim *et al.* 2005; Tong *et al.* 2024). Therefore, dysfunction of many CYP450 genes typically causes BR-deficient phenotypes, including severe dwarfism and thick, dark-green leaves (Bancoş *et al.* 2002, 2006; Zhan *et al.* 2022). Despite the high similarities between *Arabidopsis* and rapeseed, the function of those monooxygenases clarified in *Arabidopsis* have not been fully validated in rapeseed.

Using a forward screen, we isolated a dwarf mutant (*dm1*) in rapeseed and clarified that the causal genes of *dm1* are two conserved CPD/CYP90A1 genes, *BnaC09.CYP90A1* and *BnaA10.CYP90A1*. Both genes are homologous to the *Arabidopsis AtCPD/AtCYP90A1*, which encodes a CYP450 monooxygenase that catalyzes a C-3 oxidation during BR biosynthesis. Inhibiting AtCPD/AtCYP90A1 enzyme activity results in stunted plants with dense, dark-green leaves in *Arabidopsis* (Zhiponova *et al.* 2013). In our study, we demonstrated that disruption of *BnaC09.CYP90A1* and *BnaA10.CYP90A1* impairs BR biosynthesis and causes dwarfism in rapeseed through reduced cell elongation.

2. Materials and methods

2.1. Plant materials and growth conditions

The *dm1* mutant was obtained *via* the ethyl methanesulfonate (EMS) mutagenesis on the elite rapeseed line Zhongshuang 11 (ZS11). About 500 g of ZS11 seeds were immersed in 0.3% EMS solution overnight before rinsing for 10 h. Subsequently, the rinsed seeds (M_0) were sown in the field and became M_1 for selfing. In the M_2 generation, extremely dwarf mutants were selected and self-pollinated to generate an M3 population for further selection. Meanwhile, we obtained mutant *cpd* (*SALK_090732C*) from AraShare (https://www.arashare.cn/index/), which was previously developed from *AtCPD*/*At CYP90A1* in *Arabidopsis* (Guo *et al.* 2013).

For plants grown in the growth chamber, *Arabidopsis* was cultivated at 22°C–24°C with a 16-h day/8-h night cycle, under 1,800 lux light intensity, and 65% humidity. Rapeseed plants were grown in a growth room at 24°C with a 22-h day/2-h night cycle, exposed to 1,800 lux light, and maintained at 65% humidity. For the field experiment, all plants were cultivated at the experimental farm of Sichuan Agricultural University (Wenjiang, 30.70°N, 103.85°E) during the rapeseed growing season. The planting configuration in the field included a spacing of 20 cm between plants within rows and 30 cm between rows. Each line was planted in a block consisting of five rows, with approximately 10–12 plants per row. At maturity, 12–15 plants from central were harvested for the evaluation of plant architecture and agronomic traits.

2.2. Plasmid construction and plant transformation

To generate constructs for subcellular localization analysis in tobacco, the coding sequence of *BnaA10.CYP90A1* and *BnaC09.CYP90A1* and GFP protein were amplified and fused to GFP in the p1300-pUBQ10-Flag vector by cloning into the *Spe*I and *Kpn*I sites using the In-Fusion method. The Lys–Asp–Glu–Leu (KDEL) peptide and FLOURY ENDOSPERM10 (FLO10) fused to the red fluorescent protein mCherry were used as endoplasmic reticulum (ER) and mitochondria

markers for sublocalization experiments. The 35S::KDEL-mCherry, 35S::FLO10-mCherry, and 35S::NLS-mCherry constructs were kindly provided by Prof. Qin Peng (Wu *et al.* 2019). To generate the pBnaA10.CYP90A1::BnaA10.CYP90A1 construct for complementation of *dm1-s1*, a 2.0 kb promoter fragment upstream of *BnaA10.CYP90A1* was cloned together with its coding sequence into the p1300-pUBQ10-Flag vector. The constructed vector was then sent to BioRun company for further transformation into *dm1-s1*. To generate *pUBQ10::BnaA10.CYP90A1/cpd* and *pUBQ10::BnaC09.CYP90A1/cpd* transgenic lines, the constructs used for subcellular localization were introduced into heterozygous *cpd* plants by the floral dip method. In the T_1 generation, transgene-positive plants were identified, and homozygous *cpd* individuals carrying the *BnaA10.CYP90A1* or *BnaC09.CYP90A1* construct were selected in subsequent generations for propagation and phenotypic analysis. The primers listed in Appendix A were designed online (https://crm.vazyme.com/cetool/singlefragment.html).

2.3. Phenotypic characterization and agronomic trait measurement

Phenotypic characteristics, including hypocotyl length, plant height, and silique length, were measured as described in previous studies (Shi *et al.* 2019; Li *et al.* 2024). Hypocotyl length was determined using ImageJ software (https://imagej.nih.gov/ij/index.html) based on images of 7-day-old plants grown in the growth chamber. In the *BnaA10.CYP90A1/dm1-s1* complementation experiment, plant height measurements were conducted in a controlled growth chamber setting. For all other plant height measurements, they were taken in the field by determining the distance from the stem base to the tip of the main inflorescence after all flowers had withered. Silique length was measured at maturity from the central portion of the main inflorescence. Other major agronomic traits, including branch initiation height, main inflorescence length, branching number, and thousand-seed weight, were evaluated on plants harvested from the field. Additionally, seed quality was assessed using a Foss NIRSystems 5000 near-infrared reflectance spectrometer (FOSS NIRSystems, Silver Spring, MD, USA).

2.4. Cytological analysis

The embedding resin for hypocotyl and the 7th internode was prepared using the Technovit®7100 Kit (Heraeus Kulzer, Wehrheim, Germany). In short, all samples were collected and fixed in FAA fixative solution (1:2:7, acetic acid:38% formaldehyde:H_2O) for 3–7 days. Next, the samples were dehydrated in a gradient series of ethanol concentrations (70, 80, 85, 90, and 95%, and 3×100%). Following dehydration, the materials were treated with a clearing agent (1:1, ethanol:xylene) and incubated in xylene. The transparent samples were then incubated in a mixed resin solution (1:1, ethanol:Basic solution Technovit 7100) at 20°C for 2 h. For the infiltration step, an infiltration solution was prepared by mixing 1 g Hardener I with 100 mL Basic solution Technovit 7100 to infiltrate samples. The polymerization solution was prepared by combining 15 mL of infiltration medium with 1 mL of Technovit 7100 Hardener 2 for embedding the samples. The embedded samples were sectioned and observed under an Olympus BX51 microscope (Olympus, Tokyo, Japan). Cell length and width were measured from the images using ImageJ software.

2.5. Cloning of the *dm1* locus by bulk population sequencing

The *dm1* mutant was crossed with ZS11. In F_2, 30 of the most dwarf (plant height<70 cm) and 30 of the tallest plants (plant height>170 cm) were selected for bulk segregant analysis. Together with two parent lines, four pooled libraries were then prepared for sequencing using the Illumina HiSeq 2000. To identify the mutation site, sequencing reads from the bulk sample and the wild-type (WT) parent ZS11 were aligned to the ZS11 reference genome (zs11.v0, https://yanglab.hzau.edu.cn) using BWA-MEM (Yang *et al.* 2023). Next, the MutMap method (Sugihara *et al.* 2022) was employed to calculate the ΔSNP-index with default parameters.

2.6. Multiple sequence alignment and phylogenetic tree analysis

Protein identity was determined by aligning the protein sequences of AtCPD/AtCYP90A1 with six BnaCYP90A1s using MEGA 11. The final aligned result was visualized with ESPript 3.0 (Robert and Gouet 2014). For the phylogenetic tree analysis, the phylogenetic tree was built utilizing the aligned protein sequences of AtCPD/AtCYP90A1 and BnaCYP90A1s. The tree was generated using the Neighbor-Joining method through MEGA 11 software, with bootstrap parameters set at 1,000 (Kumar *et al.* 2016).

For collinearity analysis in rapeseed, comparisons between the A and C genomes were conducted using all-against-all BLASTP searches with a set e-value of 10^{-5}. For interspecies collinearity analysis, comparisons were performed using A and C genome sequences of ZS11 (zs11.v0, https://yanglab.hzau.edu.cn) as queries against *Arabidopsis* (TAIR10, https://www.Arabidopsis.org). MCScanX was used to detect tandemly duplicated genes and homologous relationships of genes in rapeseed (Wang *et al.* 2022). The evolution of *CYP90A1* in both rapeseed and *Arabidopsis* was further examined through collinearity analysis. The outcomes of these analyses were visualized using TBtools (Chen *et al.* 2020).

2.7. BL treatment

For long-term BL application, the seeds were sown on wet filter paper soaked in 200 nmol L^{-1} BL or mock solution (1:1,000, dimethyl sulfoxide (DMSO)). The hypocotyl length was determined at 5 days after sowing. For short-term BL treatment, seedlings were grown on wet filter paper for 5 days and then immersed in an aqueous solution containing 200 nmol L^{-1} BL or DMSO at a 1:1,000 dilution for 2 h. BL powder (MCE, HY-N0273) was first dissolved in DMSO to prepare a stock solution, which was then diluted 1,000-fold to obtain the working solution.

2.8. qRT-PCR and RNA-sequencing analysis

Stem tissues from mature plants and hypocotyls from 7-day-

old plants were collected for qRT-PCR analysis, respectively. Total RNA was extracted from each sample using the TRIzol reagent (Invitrogen, Carlsbad, CA, USA) method, and cDNA was synthesized using the HiScript III RT SuperMix (R323-01, Vazyme). Subsequently, the cDNA was diluted five times for qRT-PCR using a Bio-Rad CFX96 Touch Real-Time PCR Machine (Bio-Rad Laboratories, Hercules, CA, USA). Gene expression levels were normalized by $2^{-\Delta\Delta C_t}$ to the housekeeping gene, *BnaC09.UBC9*, as previously described. The primer sequences were designed by Primer Premier 5 and listed in Appendix A. All the experiments were conducted with three independent biological replicates.

For transcriptome analysis, total RNA extracted from hypocotyls was used for library construction. These libraries were sequenced on the BGIseq500 platform (BGI, Shenzhen, China). The raw data from sequencing in FASTQ format were initially processed using custom Perl scripts. The clean reads were then aligned to the ZS11 reference genome (zs11.v0, https://yanglab.hzau.edu.cn) using HISAT2. Following alignment, read counts and transcripts per million (TPM) values for each gene were calculated with StringTie2, utilizing annotation version zs11.v0. Differential expression analysis between ZS11 and *dm1* samples was conducted using the R package DESeq2, with parameters set as $\log_2|\text{Fold Change}|\geq 1$ and $P_{adj}<0.05$. To further explore and visualize the data, principal component analysis (PCA) and Pearson correlation analyses were performed using custom R scripts. All experiments were conducted with three biological replicates.

2.9. Quantification of endogenous BRs

The hypocotyls were harvested from 7-day-old plants and immediately frozen in liquid nitrogen. Next, the samples were dissolved in 1 mL acetonitrile (ACN), and 10 μL internal standard mixed solution (10 ng mL^{-1}) was added. After vortexing, the mixture was centrifuged, and then the supernatant was transferred to amber glass vials. Subsequently, 200 μL of 4-(N,N-dimethylamino) phenylboronic acid (4-DMAPBA) was added. The reaction mixture was vortexed, incubated at 75°C for 1 h, and evaporated to dryness under nitrogen. The residue was then reconstituted in 100 μL ACN and filtered through a 0.22 μm membrane filter for LC-MS/MS analysis. The content of BR was measured by MetWare (http://www.metware.cn/) using the AB Sciex QTRAP 6500 liquid chromatography tandem mass spectrometry (LC-MS/MS) platform. Data acquisition was conducted using Analyst 1.6.3 software (Sciex), and metabolite quantification was performed using Multi-quant 3.0.3 software (Sciex). Mass spectrometer parameters, such as declustering potentials (DP) and collision energies (CE) for individual MRM transitions, were optimized, and a distinct set of MRM transitions was monitored for each period based on the elution profile of metabolites during that timeframe.

2.10. Transient expression in tobacco leaves for subcellular localization analysis

The combinations of BnaA10.CYP90A1-GFP with either KDEL-mCherry (ER marker), NLS-mCherry, or FLO10-mCherry (mitochondria marker) and BnaC09.CYP90A1-GFP with either KDEL-mCherry, NLS-mCherry, or FLO10-mCherry were co-agroinfiltrated into tobacco leaves along with P19. The fluorescence signals from GFP and mCherry were visualized using a confocal laser scanning microscope (Leica STELLARIS STED, Germany) after incubation in darkness for 2 days.

2.11. Statistical analysis

All statistical analyses were conducted using GraphPad Prism v.10.2 Software. For comparing plant architecture, agronomic and quality traits, cell length and width, and gene expression between two genotypes, a two-tailed Student's unpaired *t*-test was applied. To analyze the expression patterns of *BnaCYP90A1* genes, one-way analysis of variance (ANOVA) with Tukey's multiple comparisons test was applied. In cases involving genotypes with treatments model, a two-way ANOVA was used, with Tukey's multiple comparison test employed for comparisons. Significance levels were denoted as *** for $P<0.001$, ** for $P<0.01$, and * for $P<0.05$ or denoted different significance levels with letters.

3. Results

3.1. Isolation of a dwarf mutant *dm1* in rapeseed upon EMS mutagenesis

Plant height is a pivotal rapeseed trait when determining planting density, biomass, and yield performance in the field (Hu *et al.* 2017). In this respect, we identified a dwarf mutant from an EMS treated cultivar ZS11 and named *dm1* (Fig. 1-A and B). The *dm1* mutant was 53.15% shorter ($P<0.0001$) than its WT ZS11 at maturity (Fig. 1-F). Interestingly, more than dwarfism, additional phenotypes were observed in *dm1* at different developmental stages. For example, on the 7th day after sowing, the *dm1* had 63.98% shorter hypocotyl ($P<0.0001$) than ZS11 (Fig. 1-C and G). At the bolting stage, *dm1* exhibited wrinkled and smaller petals, and flowering was delayed compared with ZS11 (Fig. 1-D). Moreover, the silique length of *dm1* was 54.11% shorter than that of ZS11 ($P<0.0001$) (Fig. 1-E and H). Additionally, the branch number, silique number, and main inflorescence length of *dm1* were significantly decreased from those of ZS11 (Appendix B). However, many important quality traits, including oil contents, glucosinolates level, and protein contents of *dm1*, were similar to those of ZS11 (Appendix B).

Because the hypocotyl length of *dm1* were tremendously shorter than those of ZS11 (Fig. 1-G), we selected the completely developed hypocotyl from 7-day-old seedlings for cytological analysis. The cell widths were similar between mutant *dm1* and its WT ZS11 in hypocotyl, whereas cell length in *dm1* was reduced by approximately 65.13% ($P<0.0001$). Next, we evaluated the length of each internode in *dm1* and ZS11 and found that the seventh internode displayed the most significant difference in length (Appendix B). Therefore, we prepared sections from the seventh internodes of *dm1* and ZS11 for cellular analysis. However, due to high fibrosis content in the nodes, we harvested the epidermal cells for comparison. Although cell width in internode epidermal cells was similar between *dm1* and ZS11, cell



Fig. 1 Phenotypic comparison between Zhongshuang 11 (ZS11) and *dm1* plants. A and B, representative plants grown in the field at the mature stage and bolting stage. Scale bar=20 cm in A and 5 cm in B. C, phenotype of 7-day-old seedlings grown in the growth chamber, scale bar=1 cm. D and E, representative flowers (D) and siliques (E) of 6-month-old plants of ZS11 and *dm1* grown in the field, scale bar=1 cm. F, plant height quantification of ZS11 and *dm1* grown in the field. In this boxplot, the central line represents the median; the whiskers span from the minimum to the maximum values; individual data points are depicted as dots, with each dot symbolizing one sample. ****, P<0.0001, Student's t-test. G, hypocotyl length measured at 7 days after stratification. Mean±SE (n=3) biological replicates with at least 30 plants per repeat per genotype. H, silique length measured on mature plants. Mean±SE (n=3) biological replicates with at least 30 siliques per repeat per genotype. ****, P<0.0001, two-way ANOVA.

length in *dm1* was reduced by 59.84% (P<0.0001) (Fig. 2). Obviously, the elongation of cells in both hypocotyl and internode was responsible for the dwarfism in *dm1*.

3.2. Identification of the causative genes for the dwarfism in *dm1*

To further determine the causative mutation of the *dm1* dwarf phenotype, we crossed the *dm1* mutant with the WT ZS11. The F_1 plants had similar sizes to their WT ZS11 after planting through to maturity (Fig. 3-A–C). Subsequently, the F_1 plants were self-pollinated to produce the F_2 generation. In the F_2 generation, 433 F_2 individuals' heights were measured; of these, 32 exhibited extreme dwarfism like *dm1*, whereas 152 were semi-dwarf and 249 were as tall as ZS11. The dwarfness:semi-dwarfness:tallness had a good fit to the 1:6:9 hypothesis, implying that mutant *dm1* was caused by two recessive genes (χ^2=1.69; P>0.05). Next, ~30 extremely dwarf or high F_2 plants were collected, respectively, for BSA. The Mutmap result located these two mutation intervals in two chromosomes of A10 and C09 (A10: 24,300,000–25,500,000; C09: 65,300,000–67,300,000) based on the Δ(single nucleotide polymorphism [SNP]-index) plot (Fig. 3-D; Appendix C). The SNPs within two regions were filtered based on the EMS-mutation type (G to A or C to T), and further filtered according to the effect of mutation on DNA/protein sequence (missense mutation or premature stop codon-gained), because the causative mutations were recessive (Chen *et al.* 2022). After being verified by polymerase chain reaction (PCR) and sequencing, eight genes were considered as candidate causal genes for *dm1* (six on A10, two on C09) (Table 1).

The respective causative genes were identified by Mutmap analysis with subsequent genetic and expression validation. The basic protein functions of the candidate genes are provided.

Next, we examined the expression of the eight candidate genes in stem tissues at the budding stage. The transcriptome data showed that all eight genes were expressed during that stage (Appendix D). Then we analyzed the linkage conditions between the SNPs in the eight genes and the *dm1* dwarf phenotype by amplifying and sequencing the SNPs in 50 extremely dwarfed F_2 plants. The sequencing results revealed that only three SNPs exhibited a 100% linkage to the *dm1* dwarfism phenotype (Fig. 3-E). Moreover, we developed KASP markers to confirm those linkages. After verifying that the KASP markers perfectly segregated the parents and F_1 genotype, we further genotyped approximately

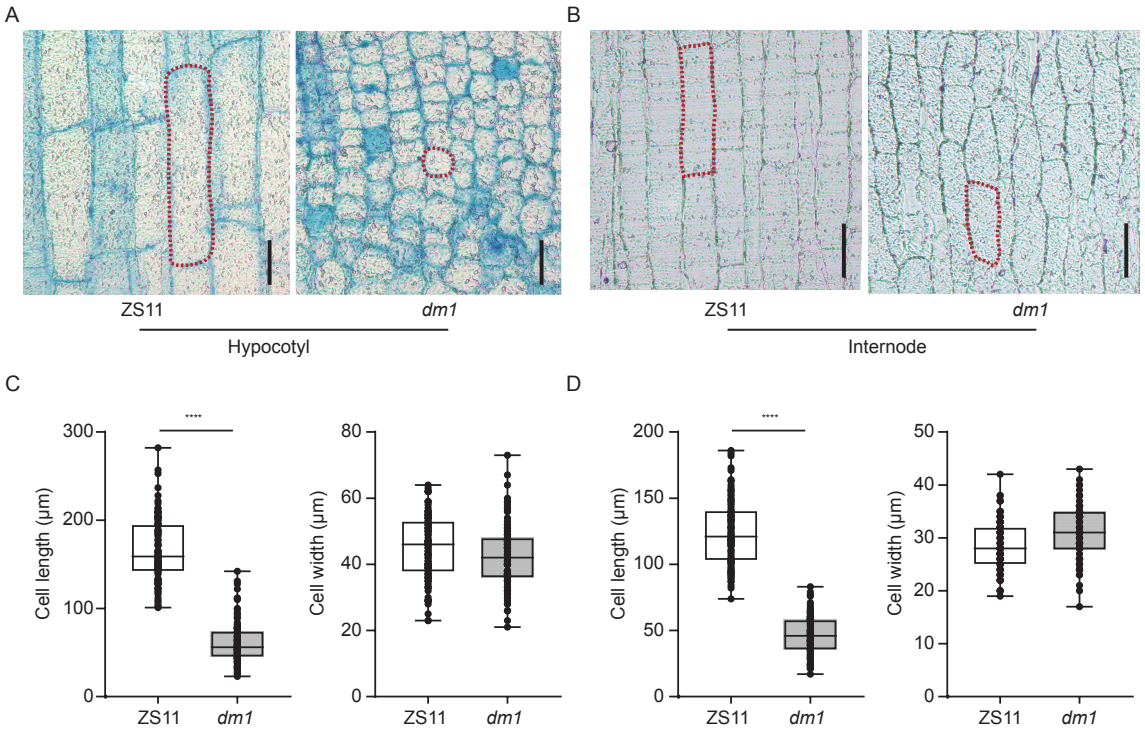


Fig. 2 Cytological observation between Zhongshuang 11 (ZS11) and *dm1* plants. A and B, hypocotyl (A) and internode epidermal cells (B) of ZS11 and *dm1*. Scale bar=100 μm. C and D, quantification of hypocotyl (C) and internode epidermal cell (D) length of the indicated lines. The central line of the boxplot represents the median; the whiskers span from the minimum to the maximum values; individual data points are depicted as dots. At least 90 cells per genotype were measured. ****, $P<0.0001$, Student's *t*-test.

40 F_2 extremely dwarf individuals. The result indicated that all tested F_2 were grouped into the mutated-genotype cluster, consolidating the association between these specific SNPs and the *dm1* dwarf phenotype (Appendix D).

Interestingly, these three SNPs were located in *BnaA10.CYP90A1* and *BnaC09.CYP90A1* genes, encoding two homologous cytochrome P450s (Gan *et al.* 2022). Of them, two SNPs were located in the coding region of *BnaA10.CYP90A1*, where the first SNP had a change from Arg27 to His27, and the second introduced a premature stop codon at Trp399. In contrast, another SNP in *BnaC09.CYP90A1* coding region caused a change from Ser120 to Phe120 (Fig. 3-F). Taken together, these results suggested that *BnaA10.CYP90A1* and *BnaC09.CYP90A1* were the most likely causative genes for the mutation of *dm1*.

3.3. *BnaA10.CYP90A1* and *BnaC09.CYP90A1* were homologous to gene *AtCPD/AtCYP90A1* and required for plant growth control

Because the functions of BnaA10.CYP90A1 and BnaC09.CYP90A1 were not reported in rapeseed, we initially performed a BLAST search of the protein sequences against the ZS11 protein database. This analysis identified six proteins sharing more than 82% sequence similarity with *BnaA10.CYP90A1* and *BnaC09.CYP90A1*, suggesting potential functional similarities (Appendix E). Interestingly, when we evaluated the expression levels of the six homologous genes in stem tissues, we discovered that, apart from *BnaA10.CYP90A1* and *BnaC09.CYP90A1*, the other four homologs were not expressed at the budding stage (Fig. 4-A). To further explore the evolution of *BnaCYP90A1* genes, we built a phylogenetic tree and conducted a collinearity analysis comparing rapeseed and *Arabidopsis* genomes. Phylogenetically, the six *BnaCYP90A1* genes were closely related to *AtCPD/AtCYP90A1*. However, based on the collinearity analysis data, only five of these genes were collineared to the *AtCPD/AtCYP90A1* gene (Fig. 4-B; Appendix E). We also performed inter-chromosomal collinearity analysis within rapeseed. The results indicated that there was no tandem duplication among *BnaCYP90A1* genes. However, we identified 14 collinear pairs within the *BnaCYP90A1* genes. The result showed that all *BnaCYP90A1* genes showed collinearity with each other, except for the *BnaC03.CYP90A1*/*BnaC09.CYP90A1* pair (Appendix E). These findings further implied that the expansion in the number of *BnCYP90A1* genes in rapeseed could be attributed to whole-genome duplication (WGD) events.

To further validate the functions of BnaA10.CYP90A1 and BnaC09.CYP90A1, we introduced *pUBQ10::BnaA10.CYP90A1-flag* and *pUBQ10::BnaC09.CYP90A1-flag* into the *Arabidopsis cpd* mutant, respectively (Fig. 4-C). As a result, these transformants from the introductions initiated the expression of *BnaC09.CYP90A1* and *BnaA10.CYP90A1*, while the endogenous *AtCPD/AtCYP90A1* expression still remained at low levels (Fig. 4-D and E). Importantly, these transformants effectively alleviated the dwarf phenotype observed in the *cpd* mutant (Fig. 4-C), indicating the crucial role of *BnaA10.CYP90A1* and *BnaC09.CYP90A1* in controlling plant growth.

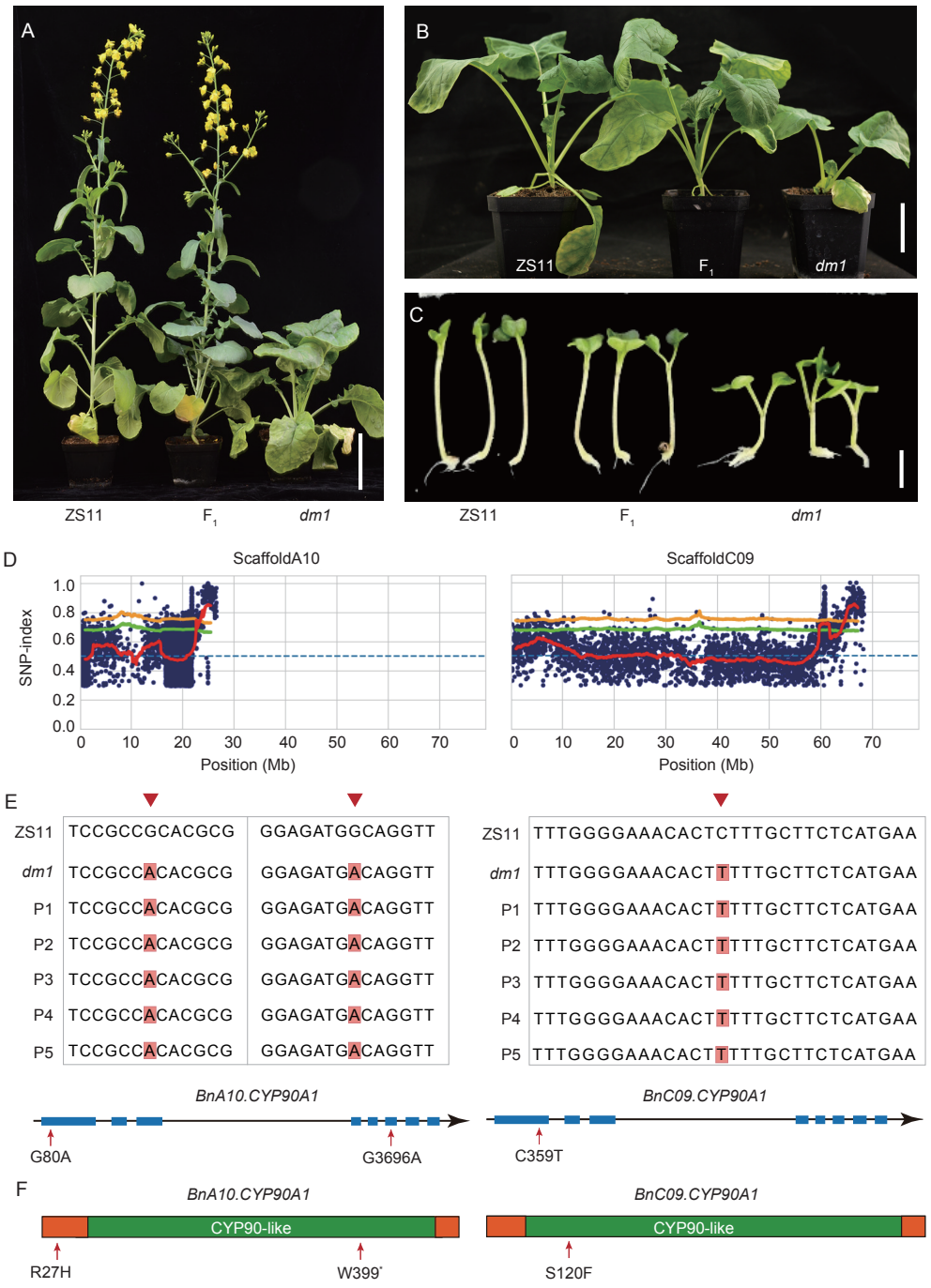


Fig. 3 Identification of causative genes for dwarfism in *dm1*. A–C, representative F_1 plants derived from the cross between Zhongshuang 11 (ZS11) and *dm1* at the mature stage, seedling stage, and 7 days after stratification. Scale bar=10 cm in A, 5 cm in B, and 0.5 cm in C. D, output of the Mutmap backcross analysis of *dm1* showing Δ(SNP-index) value of scaffoldA10 and scaffoldC09 with a clear interval. The values for other scaffolds are shown in Appendix C. E, co-segregation analysis of *dm1* dwarfism with causative SNPs. A total of 50 extremely dwarfed F_2 plants were divided into five groups (G1–G5) for sequencing with ZS11 and *dm1*. The red triangle points out the SNPs in *BnaA10.CYP90A1* and *BnaC09.CYP90A1*. The gene structures and mutation sites in *BnaA10.CYP90A1* and *BnaC09.CYP90A1* are indicated below the sequencing data. The blue rectangle represents the exon region, and the black line represents the intron region. F, position of amino acid mutations in the causative genes of *dm1*. The green rectangle represents the CYP90-like catalytic domain, the orange rectangle indicates the rest part of the protein. R, arginine; H, histidine; W, tryptophan; S, serine; F, phenylalanine. * above W399 denotes a premature stop codon.

Furthermore, we checked the expression patterns and subcellular localization of *BnaA10.CYP90A1* and *BnaC09.CYP90A1*. Various tissues from different stages were harvested for qRT-PCR measurement. The results indicated that *BnaA10.CYP90A1* exhibited higher expression in bud and stem during the budding stage (Fig. 4-F). On the other hand, *BnaC09.CYP90A1* was highly expressed in root and cotyledon during the young seedling stage, as well as in stem at the budding stage (Fig. 4-G). To determine the subcellular location of BnaA10.CYP90A1 and BnaC09.CYP90A1

Table 1 Overview of the candidate causative genes of *dm1*[1)]

Chr.	Position (bp)	Reference allele	Altered allele	Gene ID	Amino acid change[2)]	Function
A10	24,614,489	G	A	*BnaA10G0260800ZS*	Cys127Tyr	E3 ubiquitin-protein ligase
A10	24,750,057	G	A	*BnaA10G0263600ZS*	Val211Ile	Autophagy-protein 3
A10	24,873,413	G	A	*BnaA10G0265900ZS*	Glu172Lys	Thioredoxin-like 3-1
A10	24,930,972	G	A	*BnaA10G0267000ZS*	Glu305Lys	F-box protein At5g06550
A10	24,960,846	G	A	*BnaA10G0267700ZS*	His69Tyr	Ubiquitin-enzyme E1
A10	25,263,608	G	A	*BnaA10G0273600ZS*	Arg27His	Cytochrome P450 90A1
A10	25,267,224	G	A	*BnaA10G0273600ZS*	Trp399*	Cytochrome P450 90A1
C09	66,296,597	C	T	*BnaC09G0591000ZS*	Ser120Phe	Cytochrome P450 90A1
C09	66,711,372	C	T	*BnaC09G0600300ZS*	Gly161Arg	Sulfite reductase

[1)] The respective causative genes were identified by Mutmap analysis with subsequent genetic and expression validation. The basic protein functions of the candidate genes are provided

[2)] * above Trp399 denotes a premature stop codon.

proteins, the KDEL peptide, FLO10 protein, and NLS peptide were fused to the N-terminal of mCherry protein as ER, mitochondria, and nucleus marker, respectively. Both BnaA10.CYP90A1-GFP and BnaC09.CYP90A1-GFP co-localized with KDEL-mCherry, but not with NLS-mCherry or FLO10-mCherry, indicating that *BnaA10.CYP90A1* and *BnaC09.CYP90A1* are localized to the ER (Fig. 4-H).

3.4. Reduced BR levels were responsible for *dm1* dwarfism

Because *CYP90A1* encodes cytochrome P450 monooxygenase to convert 22-hydroxycampesterol (22-OHCR) into (22S,24R)-22-Hydroxy-ergost-4-en-3-one in the BR biosynthesis pathway (Ohnishi *et al.* 2012; Zhao and Li 2012), we used LC-MS/MS to measure BR contents in mutant *dm1*. It was almost impossible to simultaneously harvest the stem tissues at the same developmental stage from *dm1* and ZS11 because *dm1* flowered much later than ZS11 (Fig. 1-B). Instead, we harvested the hypocotyls from *dm1* for determining bio-active BRs content since the *dm1* hypocotyl was also shorter than ZS11's (Fig. 1-C and G). Although BL was not detected, 6-deoxoCS and CS had approximately 8- and 5-fold lower levels, respectively, in *dm1* than in ZS11 (Fig. 5-A and B). Next, we treated young seedlings of *dm1* and ZS11 with exogenous BL to determine whether the dwarfism in *dm1* could be attributed to BR deficiency. Clearly, *dm1* showed a higher sensitivity to BL compared to ZS11 plants, and the application of exogenous BL restored the shortened hypocotyl of *dm1* to the normal WT level of ZS11 (Fig. 5-C and D). Additionally, we examined the expression of BR-responsive genes in ZS11 and *dm1* after short-term BL treatment. The results indicated a clear downregulation of *BnaA01.DWF4*, *BnaC07.BR6OX2*, *BnaC07.CYP90D1*, and upregulation of *BnaC07.SAUR15* in both ZS11 and *dm1*. Importantly, the responsiveness of BR response genes was more pronounced in *dm1* (Fig. 5-E), confirming that *dm1* is more responsive to BL treatment. Collectively, these results demonstrated that the reduced levels of BRs in *dm1* should be responsible for its dwarfism.

3.5. Genes involved in BR response and cell growth were differentially expressed in *dm1*

Next, we examined whether the BR-responsive gene expression was altered in *dm1*. We profiled the transcriptome data of 7-day-old *dm1* and ZS11 hypocotyls under identical conditions. Compared to the ZS11 plants, 1,566 differentially expressed genes (DEGs) (737 up-regulated genes, 829 down-regulated genes, ($\log_2$|Fold Change|>1, P_{adj}<0.05)) were identified in *dm1* (Appendices F and G). Notably, a substantial number of the DEGs with known connections to photosynthesis, light response and hormone metabolic process were enriched in the RNA-sequencing data (Fig. 6-A).

Particularly, multiple BRs synthetic pathway genes, like *BnaROT3s*, *BnaDWF4s*, and *BnaBR6OX2s*, were upregulated in *dm1* hypocotyls, whereas the expression of *BnaBES1s*, the core members in the BR signaling pathway, were decreased in *dm1* (Fig. 6-B and D). Moreover, genes involved in cell wall synthesis/modification (Marowa *et al.* 2016; Wei *et al.* 2021; Zhu *et al.* 2023), such as *BnaC04.EXPA3*, *BnaEXP5s*, and *BnaEXP8s*, showed a clear trend of decrement in *dm1* hypocotyls (Fig. 6-C and D). We also determined the expression of these cell expansion-related genes and BR-responsive genes in stem tissues. The results clearly showed that *BnaC04.EXPA3*, *BnaC04.EXP5*, and *BnaC07.SAUR15* were expressed at much lower levels in stem tissues of *dm1* than those of ZS11 (Fig. 6-E). Overall, these results indicated that most genes associated with BR response and cell growth had a lower expression level in *dm1*.

3.6. Single mutation and haplotype analysis of *BnaA10.CYP90A1*

Given that the double mutations of *BnaA10.CYP90A1* and *BnaC09.CYP90A1* severely disrupted the architecture of *dm1*, we proposed whether a single mutation in *BnaA10.CYP90A1* could confer a semi-dwarf phenotype. To test this hypothesis, we isolated the *BnaA10.CYP90A1* single mutant, and designated it as *dm1-s1*, from F_2 plants generated by *dm1* and ZS11 crosses (Appendix H). The *dm1-s1* plants displayed a semi-dwarf phenotype, with its siliques being slightly shorter and fewer in number than those of ZS11 (Fig. 7-A–F; Appendix H). To verify whether the mutation of *BnaA10.CYP90A1* is responsible for the semi-dwarfism in *dm1-s1*, we introduced the *pBnaA10.CYP90A1::BnaA10.CYP90A1* construct into the *dm1-s1* single mutant. At the first generation of transformants, 10 positive transformants restored the *dm1-s1* semi-dwarf phenotype (Fig. 7-G and

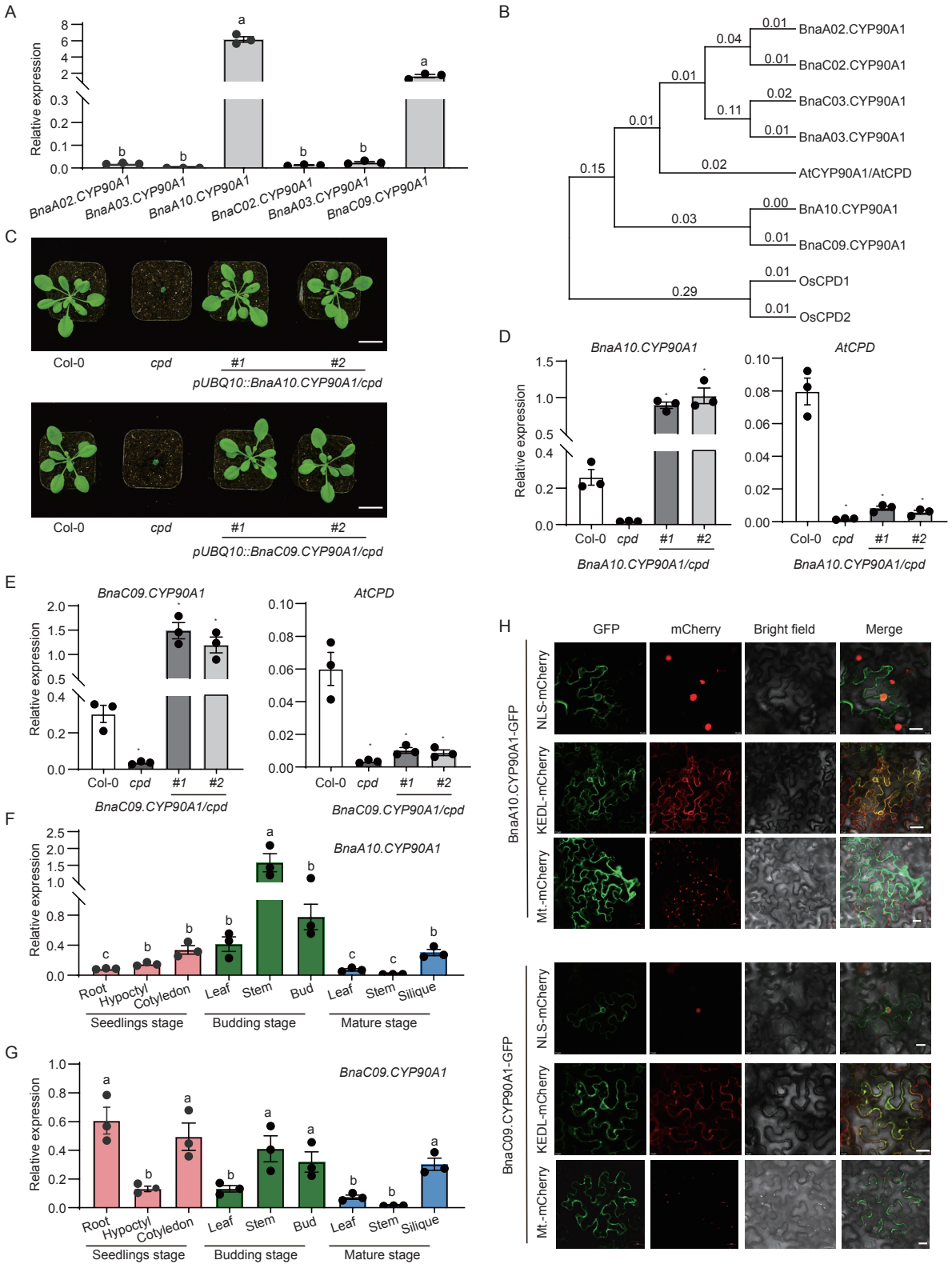


Fig. 4 *BnaA10.CYP90A1* and *BnaC09.CYP90A1* were required for plant growth control. A, the expression of six *BnaCYP90A1* genes in the stem tissues at the budding stage. Bars mean SE (n=3 biological replicates). One-way ANOVA with Tukey multiple comparison test was applied for significant analysis. Different letters represent significant differences (P<0.05). B, phylogenetic tree of *CYP90A1* homologs from rapeseed, rice, and *Arabidopsis*. C, phenotype of *cpd* complemented with *pUBQ10::BnaA10.CYP90A1* or *pUBQ10::BnaC09.CYP90A1*. Scale bar=2 cm. D and E, expression of *AtCPD/AtCYP90A1*, *BnaA10.CYP90A1*, and *BnaC09.CYP90A1* in Col-0, *cpd*, and complement lines, respectively. Bars mean SE (n=3 biological replicates). *, P<0.05, student's t-test. F and G, the expression pattern of *BnaA10.CYP90A1* and *BnaC09.CYP90A1* in different tissues. Bars mean SE (n=3 biological replicates). One-way ANOVA with Tukey multiple comparison test was applied for significant analysis. Different letters represent significant differences (P<0.05). H, subcellular localization of BnaA10.CYP90A1-GFP and BnaC09.CYP90A1-GFP protein in *Nicotiana benthamiana* epidermal cells. Individual images of green fluorescent protein (GFP) or mCherry are shown. GFP or mCherry merged with bright field images were also shown. Mt. stands for mitochondria. Scale bar=20 μm.

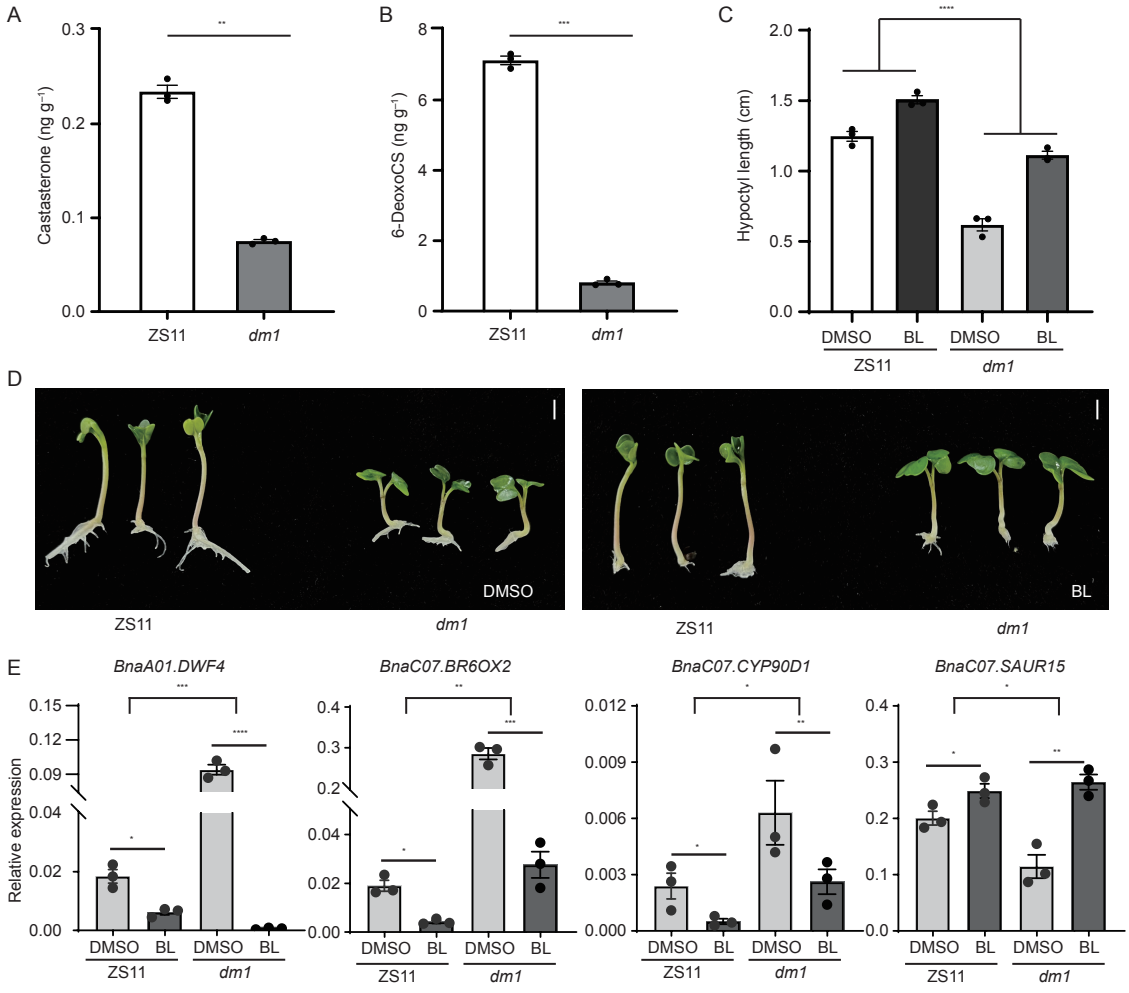


Fig. 5 Recovery of the *dm1* shortened hypocotyl by exogenous application of brassinolide (BL). A and B, castasterone (A) and 6-deoxocastasterone (6-deoxoCS) (B) levels in Zhongshuang 11 (ZS11) and *dm1*. Mean±SE (n=3). **, P<0.01; ***, P<0.001, Student's t-test. C, hypocotyl length of 5-day-old seedlings treated with 200 nmol L^{-1} BL or 0.1% dimethyl sulfoxide (DMSO) (n=3), biological replicates with at least 30 seedlings per genotype per replicate. Asterisks represent P-values of two-way ANOVA genotype×treatment interaction test, ****, P<0.0001. D, representative plants of 5-day-old seedlings of the indicated genotypes under BL treatment or 0.1% DMSO condition. Scale bar=5 mm. E, expression of brassinosteroid (BR)-responsive genes after short-term BL treatment. Bars mean SE (n=3 biological replicates). Student's t-test was used to compare treatment effects, and two-way ANOVA was used to evaluate genotype×treatment interaction test. *, P<0.05; **, P<0.01; ***, P<0.001; ****, P<0.0001.

H), suggesting that *BnaA10.CYP90A1* could regulate plant height alone in rapeseed.

Next, we performed a haplotype analysis on *BnaA10.CYP90A1* in the natural population resources. Six haplotypes (Hap0–Hap5) were identified based on sequencing data of nature population resources derived from BnIR (https://yanglab.hzau.edu.cn/) (Yang *et al.* 2023). Among six haplotypes, most of the mutations happened in the promoter region with single nucleotide substitutions. One exception was noted in Hap3, where 14 bp were missing in the promoter region (Fig. 8-A). In addition, according to the phenotypic data in BnIR, Hap4 showed a clear reduction in plant height in comparison with the other five haplotypes (Sun *et al.* 2016) (Appendix H). In contrast to *BnaA10.CYP90A1*, there are 3 haplotypes in *BnaC09.CYP90A1*, among which Hap0 and Hap2 are nearly identical except for one SNP in the first intron. Hap1 showed several amino acid differences (Fig. 8-B) and exhibited a clearly higher proportion in spring rapeseed (Appendix H). Overall, these results highlight a greater diversity in haplotypes observed within *BnaA10.CYP90A1*.

4. Discussion

4.1. *BnaA10.CYP90A1* and *BnaC09.CYP90A1* are key BR biosynthetic genes controlling plant height in rapeseed

BRs represent a class of steroid hormones crucial for various aspects of plant growth and development, encompassing cell elongation, division, photomorphogenesis, and reproduction (Gudesblat and Russinova 2011; Kim and Russinova 2020). In rapeseed, previous studies have confirmed the importance of BR signaling components, such as *BnaBRI1*, *BnaBIN2s*, and *BnaC04.BIL1*, in plant height regulation (Yang *et al.* 2021; Song *et al.* 2022; Li *et al.* 2023). However, except for the role of BnaC07.ROT3 (Zhou *et al.* 2022), the precise role of the BR biosynthetic pathway in rapeseed remains unclear.

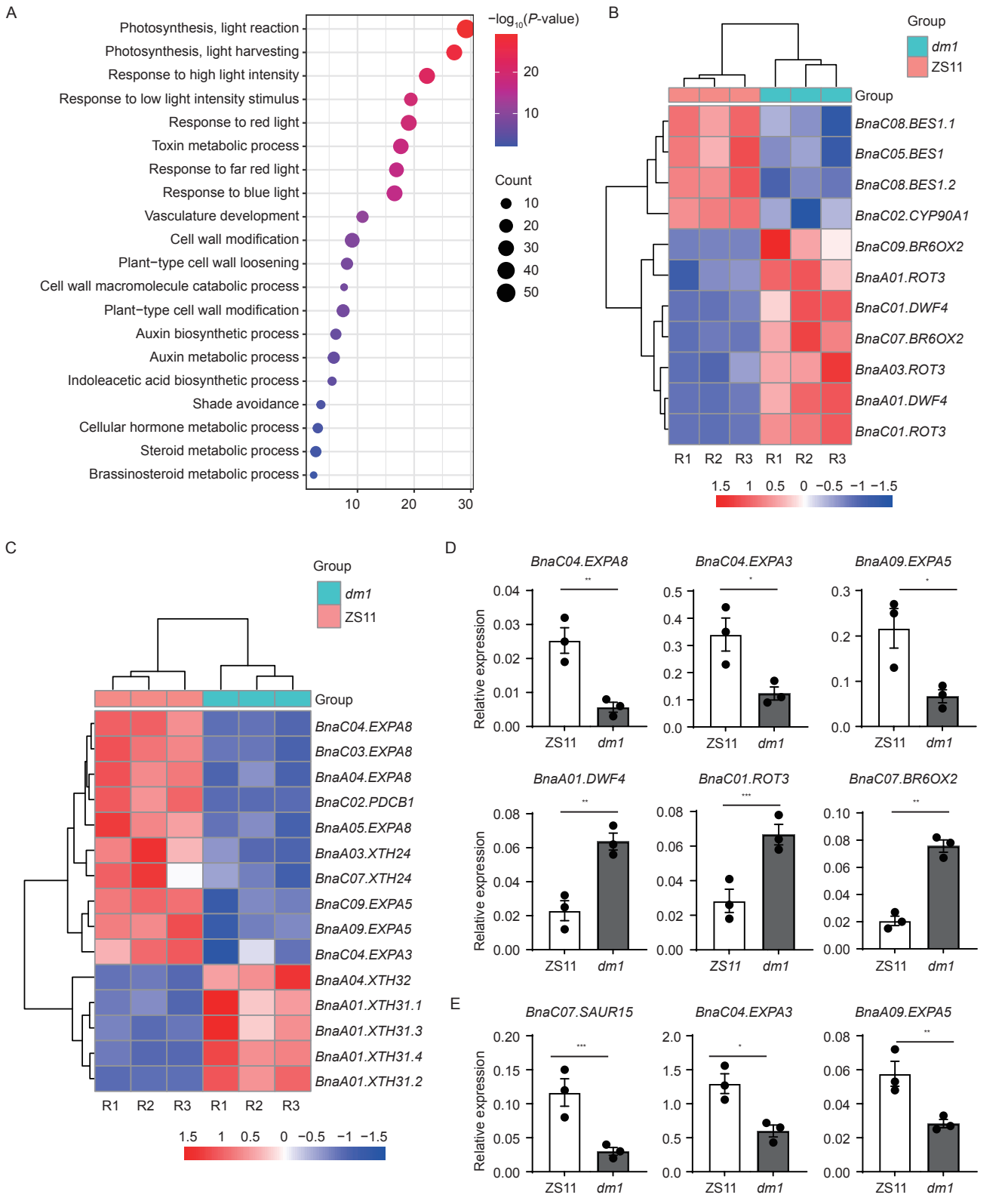


Fig. 6 Transcriptome analysis of Zhongshuang 11 (ZS11) and *dm1*. A, Gene Ontology enrichment for differentially expressed genes (DEGs) between ZS11 and *dm1*. B and C, heatmap of expression profiles of DEGs involved in the brassinosteroid (BR) biosynthesis and signaling transduction (B), and cell wall modification (C). R1–R3 indicate three biological replicates. D and E, expression analysis *via* qRT-PCR quantifying transcript levels of genes involved in BR-biosynthesis and cell wall modification in hypocotyl (D) and stem tissues (E). Bars mean SE (n=3 biological replicates). *, P<0.05; **, P<0.01; ***, P<0.001, Student's t-test.

In this study, we isolated an extremely dwarf mutant, *dm1*, from the mutagenesis of EMS. The *dm1* plants displayed a series of typical BR-deficient phenotypes, including markedly shortened hypocotyls, small dark-green leaves, and wrinkled

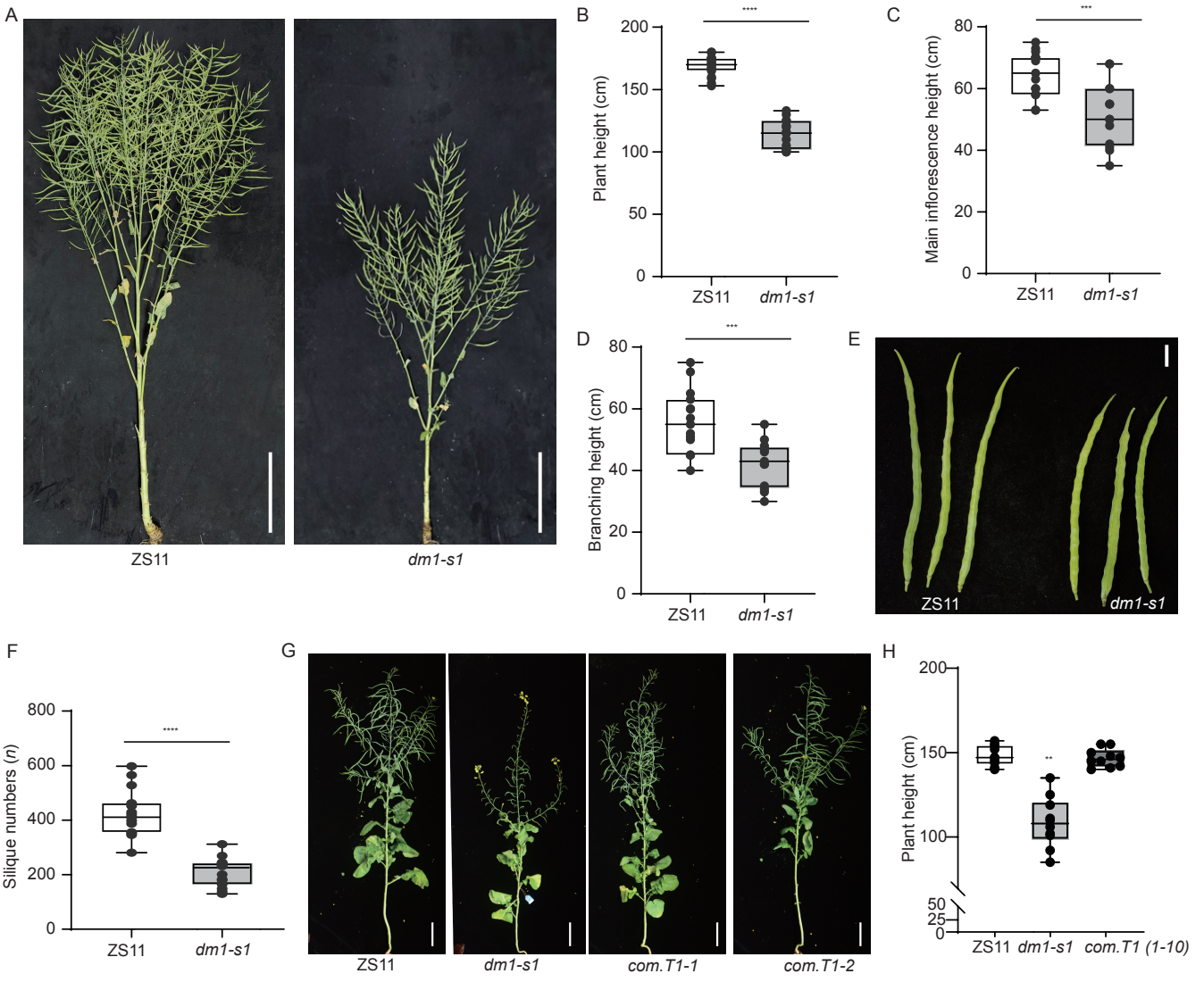


Fig. 7 Effects of the single *BnaA10.CYP90A1* mutation in *dm1-s1*. A, morphology of Zhongshuang 11 (ZS11) and *dm1-s1* plants grown in the field at the mature stage. Scale bar=10 cm. B–D, quantification of plant height (B), main inflorescence length (C), and branch height (D) of ZS11 and *dm1-s1*. Within the boxplot, the median is indicated by the central line, the whiskers extend from the minimum to the maximum values, with each individual data point represented as a dot. ***, $P<0.001$; ****, $P<0.0001$, Student's *t*-test. E, representative siliques of ZS11 and *dm1-s1*. Scale bar=1 cm. F, silique numbers counted in mature plants of the mentioned lines. Bars mean SE ($n=3$ biological replicates) and at least 30 siliques per repeat per genotype. Statistical significance is indicated by **** ($P<0.0001$), determined using a two-way ANOVA analysis. G, phenotypes of T1 transgenic lines carrying *pBnaA10.CYP90A1::BnaA10.CYP90A1* in the *dm1-s1* background. *com.T1* stands for the abbreviation of complement T1 lines. Scale bar=10 cm. H, plant height quantification of ZS11, *dm1-s1*, and T1 complement lines shown in G. In this boxplot, the central line represents the median; the whiskers span from the minimum to the maximum values; individual data points are depicted as dots, with each dot symbolizing one sample. **, $P<0.01$, Student's *t*-test.

flowers (Fig. 1-A–E). We pinpointed *BnaA10.CYP90A1* and *BnaC09.CYP90A1* as the causal genes for the dwarfism of *dm1*. The premature stop codon in *BnaA10.CYP90A1* and the S120F substitution in *BnaC09.CYP90A1* likely impair the biochemical functions of these proteins, as both mutations occur at conserved amino acid residues within the CYP90-like domain (Appendix D).

Both *BnaA10.CYP90A1* and *BnaC09.CYP90A1* are homologous to *AtCPD/AtCYP90A1* in *Arabidopsis*. So far, only the *AtCPD/AtCYP90A1* gene has been extensively characterized through mutant screens and metabolite profiling (Ohnishi *et al.* 2012). It was reported that AtCPD/AtCYP90A1 is involved in mediating the C-3 oxidation of CN and 22-OHCR to promote BR biosynthesis. Therefore, the loss-of-function *cpd* mutant displayed extreme growth defects. In our studies, introducing *BnaA10.CYP90A1* and *BnaC09.CYP90A1* into the *AtCPD/AtCYP90A1* mutant *cpd* significantly reversed its dwarf phenotype (Fig. 4-C), underlining their similar function with *AtCPD/AtCYP90A1* and crucial roles in plant growth control. Accordingly, the amounts of bioactive BR and CS were significantly diminished in the *dm1* hypocotyl (Fig. 5-A and B). Although other bioactive BRs were not detected, exogenous BL restored hypocotyl elongation in *dm1* to nearly the WT level (Fig. 5-C). Furthermore, multiple BR synthetic pathway core genes were upregulated in *dm1*, which might be due to a feedback

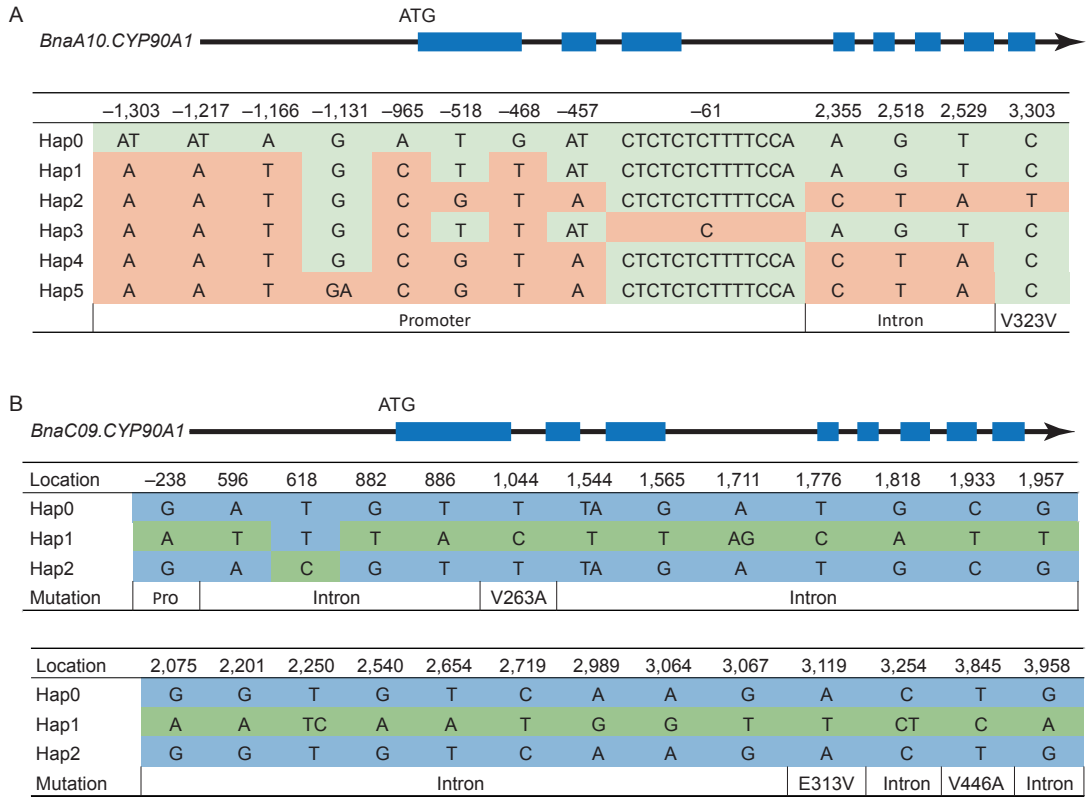


Fig. 8 Haplotype analysis of *BnaC09.CYP90A1* and *BnaA10.CYP90A1*. The gene structure and allelic variation on *BnaA10.CYP90A1* (A) and *BnaC09.CYP90A1* (B) were shown based on SNP data from the BnIR database (https://yanglab.hzau.edu.cn/BnIR).

regulation for the classical BR biosynthesis (Zhao and Li 2012). Therefore, these results demonstrate that the reduced BR level in *dm1* is responsible for its dwarf phenotype.

4.2. Reduced BR accumulation in *dm1* restricts cell elongation and alters downstream growth-related pathways

Plant height is determined by the coordinated regulation of cell elongation, cell division, and tissue differentiation, all of which together shape overall plant architecture (Wolf 2022; Cosgrove 2024). In the hypocotyl and stem tissues of *dm1*, we observed a clear reduction in cell size, particularly in cell length (Fig. 2), indicating that impaired cell elongation is a major cellular basis for the dwarf phenotype. This reduction in cell length is likely associated with the downregulation of several cell expansion-related genes, including *BnaEXPA3*, *BnaEXPA5s*, and *BnaEXPA8s* (Fig. 6-C–E). Because these genes are involved in cell wall loosening and elongation, their reduced expression provides a plausible molecular explanation for the suppressed cell expansion observed in *dm1*. Therefore, BR deficiency caused by loss of *BnaCYP90A1* function likely restricts plant growth at least in part by repressing genes required for cell elongation.

In addition to the cell expansion-related genes, genes involved in auxin biosynthesis and metabolism were also differentially expressed in *dm1*. Therefore, we speculated that the BRs deficiency might affect auxin levels in *dm1*. Consequently, BRs and auxin together impact various processes of cell construction in *dm1*. Moreover, a large number of genes associated with light response were also altered in *dm1*. These include genes encoding light-responsive transcription factors such as B-BOX DOMAIN PROTEIN 18 (BnaA02.BBX18), PHYTOCHROME-INTERACTING FACTOR 5 (BnaC05.PIF5), and chlorophyll a-b binding proteins like LIGHT-HARVESTING CHLOROPHYLL B-BINDING 1 (BnaA03.LHCB1) and BnaA05.LHCB4.3 (Zhang and Lin 2017; Pham *et al.* 2018; Vayghan *et al.* 2022). In *Arabidopsis*, BR-deficient mutants often exhibit typical photomorphogenic traits in darkness, such as shortened hypocotyls and opened cotyledons, highlighting the close relationship between light signaling and BR pathways. This connection may also be conserved in rapeseed, given the similar photomorphogenic phenotype observed in *dm1* during the young seedling stage. Overall, this observation implies a possible interconnection between auxin, light, and BR signals, contributing to the precise regulation of plant growth and development in rapeseed.

4.3. The *BnaCYP90A1* gene family has expanded and functionally diverged in rapeseed

Unlike the single copy of the *CYP90A1* gene in *Arabidopsis*, there are six *BnaCYP90A1* genes in rapeseed (Fig. 4-B). This expansion is likely the result of whole-genome duplication events, as suggested by the extensive collinearity relationships within the rapeseed genome and the absence of tandem duplication among *BnaCYP90A1* genes.

Nevertheless, not all copies appear to contribute equally to stem growth regulation. Among the six homologs, only *BnaA10.CYP90A1* and *BnaC09.CYP90A1* were expressed in stem tissues at the budding stage (Fig. 4-A), indicating that these two copies likely play predominant roles in controlling stem elongation at this developmental stage.

Variation in *CPD/CYP90A1* copy number is also evident across plant species. In addition to the expanded copy number in rapeseed, previous studies have shown that the number of *CPD* homologs differs among crops, suggesting lineage-specific retention and divergence following genome duplication events (Zebosi *et al.* 2024). Apart from the gene copy numbers, subcellular localization of CPD proteins also varies. Our study validated that BnaA10.CYP90A1 and BnaC09.CYP90A1 are located in the ER, similar to the OsCPD proteins (Zhan *et al.* 2022), while AtCPD/AtCYP90A1 was reported to be not only located in ER but also in mitochondria (Bellido *et al.* 2022; Wang *et al.* 2023). This difference in subcellular localization may have functional consequences, because *AtCPD/AtCYP90A1* was shown to interact with mitochondrial adrenodoxins during ovule development. Therefore, the coexistence of multiple *BnaCYP90A1* homologs in rapeseed may reflect functional diversification in BR metabolism across tissues or developmental contexts. In particular, the remaining four *BnaCYP90A1* homologs, which were not expressed in stems at the budding stage, may exhibit distinct expression domains or subcellular localizations, and this possibility deserves further investigation.

4.4. *BnaA10.CYP90A1* is a promising but challenging target for semi-dwarf breeding in rapeseed

More importantly, the *dm1-s1* mutant, which carries a mutation in *BnaA10.CYP90A1* but not in *BnaC09.CYP90A1*, displayed a semi-dwarf phenotype in rapeseed (Fig. 7). This result indicates that partial disruption of *BnaCYP90A1* function can reduce plant height without causing the severe developmental defects observed in the double mutant *dm1*. From a breeding perspective, this finding is important because reduced plant height is often desirable for lodging resistance and cultivation management. However, the breeding value of *dm1-s1* is not straightforward. Although its semi-dwarf stature may be favorable, the accompanying reduction in branch number and silique length makes this mutant less suitable for direct breeding use.

To exploit the semi-dwarf phenotype while minimizing undesirable side effects, a more practical strategy may be to fine-tune *BnaA10.CYP90A1* function rather than completely disrupt it. For example, promoter editing using the CRISPR/Cas9 system could be used to moderately reduce *BnaA10.CYP90A1* expression and thereby generate elite semi-dwarf germplasm with fewer penalties on agronomic traits. Natural variation may provide another promising route. In the sequenced natural population, six haplotypes were identified for *BnaA10.CYP90A1*, with most polymorphisms located in the promoter region. In particular, Hap3 contains a 14-bp deletion in the promoter (Fig. 8-A), making it a promising candidate for further analysis of promoter activity and breeding potential. In addition, weakened *BnaA10.CYP90A1* alleles may be combined with other genetic resources that enhance vegetative growth, which may help reduce plant height while buffering negative effects on branching and silique development. Finally, because *dm1-s1* exhibits a more compact architecture, increasing planting density may help improve harvest index without substantially compromising yield. Overall, these strategies highlight the potential of *BnaA10.CYP90A1* as a target for semi-dwarf breeding, while also emphasizing that its effective use will likely require precise modulation rather than complete loss of function.

5. Conclusion

In this study, we identified two cytochrome P450 genes, *BnaC09.CYP90A1* and *BnaA10.CYP90A1*, as the causal genes underlying the dwarf phenotype of the novel EMS mutant *dm1*. We demonstrated that both genes are involved in BR biosynthesis and play essential roles in plant growth regulation. Cellular and molecular analyses further revealed that loss of *BnaC09.CYP90A1* and *BnaA10.CYP90A1* function impairs cell elongation, thereby reducing plant height. Notably, a single mutation in *BnaA10.CYP90A1* conferred a semi-dwarf rather than extreme dwarf phenotype, highlighting its potential value for rapeseed ideotype improvement and cultivar development.

Acknowledgements

This work was supported by the Science and Technology Innovation 2030-Major Project, China (2023ZD04069), the Natural Science Foundation of Sichuan Province, China (23NSFSC0765), the Postdoctoral Fellowship Program of China Postdoctoral Science Foundation (GZB20230498), the Key Research and Development Projects of Chengdu, China (2023-YF09-00024-SN), and the Sichuan Innovation Team Project, China (SCCXTD-2024-3). We thank the High-performance Computing Platform of Sichuan Agricultural University for their support for the RNA sequencing. We are also grateful to Profs. Peng Qin, Xuewei Cheng, Shigui Li, and Wenming Wang, Drs. Yaowei Wang and Jiaowei Xiong (Sichuan Agricultural University), for fruitful discussions and/or sharing of plant material and plasmid, Liangzhu Kang (Sichuan Agricultural University) for all the practical help, and Prof. Wengui Yan (Sichuan Agricultural University) for critically reading and improving the manuscript.

Declaration of competing interest

The authors declare that they have no conflict of interest.

Declaration of generative AI and AI-assisted technologies in the writing process

During the preparation of this manuscript, the authors used ChatGPT 5.2 to assist in improving the clarity and readability of the language. All content generated was carefully reviewed and revised by the authors as necessary, and the authors take full responsibility for the final content of the article.

Data availability

All data and materials integral to the paper are available to

readers upon request to the authors. The RNA sequencing data are available on National Genomics Data Center (https://ngdc.cncb.ac.cn/).

Appendices associated with this paper are available at https://doi.org/10.1016/j.jia.2024.12.016

References

Achard P, Gusti A, Cheminant S, Alioua M, Dhondt S, Coppens F, Beemster G T, Genschik P. 2009. Gibberellin signaling controls cell proliferation rate in *Arabidopsis*. *Current Biology*, **19**, 1188–1193.

Bancoş S, Nomura T, Sato T, Molnár G, Bishop G J, Koncz C, Yokota T, Nagy F, Szekeres M. 2002. Regulation of transcript levels of the *Arabidopsis* cytochrome P450 genes involved in brassinosteroid biosynthesis. *Plant Physiology*, **130**, 504–513.

Bancos S, Szatmári A M, Castle J, Kozma-Bognár L, Shibata K, Yokota T, Bishop G J, Nagy F, Szekeres M. 2006. Diurnal regulation of the brassinosteroid-biosynthetic CPD gene in *Arabidopsis*. *Plant Physiology*, **141**, 299–309.

Bellido A M, Distéfano A M, Setzes N, Cascallares M M, Oklestkova J, Novak O, Ramirez J A, Zabaleta E J, Fiol D F, Pagnussat G C. 2022. A mitochondrial ADXR-ADX-P450 electron transport chain is essential for maternal gametophytic control of embryogenesis in *Arabidopsis*. *Proceedings of the National Academy of Sciences of the United States of America*, **119**, e2000482119.

Chen C, Chen H, Zhang Y, Thomas H R, Frank M H, He Y, Xia R. 2020. TBtools: An integrative toolkit developed for interactive analyses of big biological data. *Molecular Plant*, **13**, 1194–1202.

Chen L, Duan L, Sun M, Yang Z, Li H, Hu K, Yang H, Liu L. 2022. Current trends and insights on EMS mutagenesis application to studies on plant abiotic stress tolerance and development. *Frontiers in Plant Science*, **13**, 1052569.

Chen X, Hu X, Jiang J, Wang X. 2024. Functions and mechanisms of brassinosteroids in regulating crop agronomic traits. *Plant and Cell Physiology*, **65**, 1568–1580.

Cheng H, Jin F, Zaman Q U, Ding B, Hao M, Wang Y, Huang Y, Wells R, Dong Y, Hu Q. 2019. Identification of *Bna.IAA7.C05* as allelic gene for dwarf mutant generated from tissue culture in oilseed rape. *BMC Plant Biology*, **19**, 500.

Cosgrove D J. 2024. Structure and growth of plant cell walls. *Nature Reviews Molecular Cell Biology*, **25**, 340–358.

Du X, Hussain N, Li Z, Chen X, Hua S, Zhang D, Jiang L. 2015. Effect of gibberellin on the biosynthesis of tocopherols in oilseed rape (*Brassica napus* L.) and *Arabidopsis*. *Journal of Agricultural and Food Chemistry*, **63**, 360–369.

Gan Q, Luan M, Hu M, Liu Z, Zhang Z. 2022. Functional study of *CYP90A1* and *ALDH3F1* gene obtained by transcriptome sequencing analysis of *Brassica napus* seedlings treated with brassinolide. *Frontiers in Plant Science*, **13**, 1040511.

Gao J, Qin P, Tang S, Guo L, Dai C, Wen J, Yi B, Ma C, Shen J, Fu T, Zou J, Tu J. 2024. A gain-of-function mutation in *BnaIAA13* disrupts vascular tissue and lateral root development in *Brassica napus*. *Journal of Experimental Botany*, **75**, 5592–5610.

Gudesblat G E, Russinova E. 2011. Plants grow on brassinosteroids. *Current Opinion in Plant Biology*, **14**, 530–537.

Guo R, Qian H, Shen W, Liu L, Zhang M, Cai C, Zhao Y, Qiao J, Wang Q. 2013. BZR1 and BES1 participate in regulation of glucosinolate biosynthesis by brassinosteroids in *Arabidopsis*. *Journal of Experimental Botany*, **64**, 2401–2412.

Hong Z, Ueguchi-Tanaka M, Fujioka S, Takatsuto S, Yoshida S, Hasegawa Y, Ashikari M, Kitano H, Matsuoka M. 2005. The rice brassinosteroid-deficient *dwarf2* mutant, defective in the rice homolog of *Arabidopsis* DIMINUTO/DWARF1, is rescued by the endogenously accumulated alternative bioactive brassinosteroid, dolichosterone. *The Plant Cell*, **17**, 2243–2254.

Hu D, Jing J, Snowdon R J, Mason A S, Shen J, Meng J, Zou J. 2021. Exploring the gene pool of *Brassica napus* by genomics-based approaches. *Plant Biotechnology Journal*, **19**, 1693–1712.

Hu Q, Hua W, Yin Y, Zhang X, Liu L, Shi J, Zhao Y, Qin L, Chen C, Wang H. 2017. Rapeseed research and production in China. *The Crop Journal*, **5**, 127–135.

Kim E J, Russinova E. 2020. Brassinosteroid signalling. *Current Biology*, **30**, R294–R298.

Kim G T, Tsukaya H, Uchimiya H. 1998. The *ROTUNDIFOLIA3* gene of *Arabidopsis* thaliana encodes a new member of the cytochrome P-450 family that is required for the regulated polar elongation of leaf cells. *Genes & Development*, **12**, 2381–2391.

Kim H B, Kwon M, Ryu H, Fujioka S, Takatsuto S, Yoshida S, An C S, Lee I, Hwang I, Choe S. 2006. The regulation of DWARF4 expression is likely a critical mechanism in maintaining the homeostasis of bioactive brassinosteroids in *Arabidopsis*. *Plant Physiology*, **140**, 548–557.

Kim T W, Hwang J Y, Kim Y S, Joo S H, Chang S C, Lee J S, Takatsuto S, Kim S K. 2005. *Arabidopsis* CYP85A2, a cytochrome P450, mediates the Baeyer-Villiger oxidation of castasterone to brassinolide in brassinosteroid biosynthesis. *The Plant Cell*, **17**, 2397–2412.

Kumar S, Stecher G, Tamura K. 2016. MEGA7: Molecular evolutionary genetics analysis version 7.0 for bigger datasets. *Molecular Biology and Evolution*, **33**, 1870–1874.

Li B, Liu X, Guo Y, Deng L, Qu L, Yan M, Li M, Wang T. 2023. BnaC01.BIN2, a GSK3-like kinase, modulates plant height and yield potential in *Brassica napus*. *Theoretical and Applied Genetics*, **136**, 29.

Li H, Li J, Song J, Zhao B, Guo C, Wang B, Zhang Q, Wang J, King G J, Liu K. 2019. An auxin signaling gene *BnaA3.IAA7* contributes to improved plant architecture and yield heterosis in rapeseed. *New Phytologist*, **222**, 837–851.

Li T, Wang Y, Natran A, Zhang Y, Wang H, Du K, Qin P, Yuan H, Chen W, Tu B, Inzé D, Dubois M. 2024. C-TERMINAL DOMAIN PHOSPHATASE-LIKE 3 contributes to GA-mediated growth and flowering by interaction with DELLA proteins. *New Phytologist*, **242**, 2555–2569.

Liu C, Wang J, Huang T, Wang F, Yuan F, Cheng X, Zhang Y, Shi S, Wu J, Liu K. 2010. A missense mutation in the VHYNP motif of a DELLA protein causes a semi-dwarf mutant phenotype in *Brassica napus*. *Theoretical and Applied Genetics*, **121**, 249–258.

Liu S, Raman H, Xiang Y, Zhao C, Huang J, Zhang Y. 2022. *De novo* design of future rapeseed crops: Challenges and opportunities. *The Crop Journal*, **10**, 587–596.

Marowa P, Ding A, Kong Y. 2016. Expansins: Roles in plant growth and potential applications in crop improvement. *Plant Cell Reports*, **35**, 949–965.

Noguchi T, Fujioka S, Takatsuto S, Sakurai A, Yoshida S, Li J, Chory J. 1999. *Arabidopsis* det2 is defective in the conversion of (24R)–24-methylcholest-4-En-3-one to (24R)-24-methyl-5alpha-cholestan-3-one in brassinosteroid biosynthesis. *Plant Physiology*, **120**, 833–840.

Ohnishi T, Godza B, Watanabe B, Fujioka S, Hategan L, Ide K, Shibata K, Yokota T, Szekeres M, Mizutani M. 2012. CYP90A1/CPD, a brassinosteroid biosynthetic cytochrome P450 of *Arabidopsis*, catalyzes C-3 oxidation. *Journal of Biological Chemistry*, **287**, 31551–31560.

Pham V N, Kathare P K, Huq E. 2018. Dynamic regulation of PIF5 by COP1-SPA complex to optimize photomorphogenesis in *Arabidopsis*. *The Plant Journal*, **96**, 260–273.

Ping X, Ye Q, Yan M, Zeng J, Yan X, Li H, Li J, Liu L. 2022. Integrated genetic mapping and transcriptome analysis reveal the BnaA03.IAA7 protein regulates plant architecture and gibberellin signaling in *Brassica napus* L. *Theoretical and Applied Genetics*, **135**, 3497–3510.

Robert X, Gouet P. 2014. Deciphering key features in protein structures with the new ENDscript server. *Nucleic Acids Research*, **42**, W320–W324.

Shi L, Song J, Guo C, Wang B, Guan Z, Yang P, Chen X, Zhang Q, King G J, Wang J, Liu K. 2019. A CACTA-like transposable element in the upstream region of *BnaA9.CYP78A9* acts as an enhancer to increase silique length and seed weight in rapeseed. *The Plant Journal*, **98**, 524–539.

Song L, Liu J, Cao B, Liu B, Zhang X, Chen Z, Dong C, Liu X, Zhang Z, Wang W, Chai L, Liu J, Zhu J, Cui S, He F, Peng H, Hu Z, Su Z, Guo W, Xin M, *et al.* 2023. Reducing brassinosteroid signalling enhances grain yield in semi-dwarf wheat. *Nature*, **617**, 118–124.

Song M, Linghu B, Huang S, Li F, An R, Xie C, Zhu Y, Hu S, Mu J, Zhang Y. 2022. Genome-wide survey of leucine-rich repeat receptor-like protein kinase genes and CRISPR/Cas9-targeted mutagenesis BnBRI1 in *Brassica napus*. *Frontiers in Plant Science*, **13**, 865132.

Sugihara Y, Young L, Yaegashi H, Natsume S, Shea D J, Takagi H, Booker H, Innan H, Terauchi R, Abe A. 2022. High-performance pipeline for MutMap and QTL-seq. *PeerJ*, **10**, e13170.

Sun C, Wang B, Yan L, Hu K, Liu S, Zhou Y, Guan C, Zhang Z, Li J, Zhang J, Chen S, Wen J, Ma C, Tu J, Shen J, Fu T, Yi B. 2016. Genome-wide association study provides insight into the genetic control of plant height in rapeseed (*Brassica napus* L.). *Frontiers in Plant Science*, **7**, 1102.

Tong J, Zhao W, Wang K, Deng D, Xiao L. 2024. Organ-level distribution tandem mass spectrometry analysis of three structural types of brassinosteroids in rapeseed. *Frontiers in Plant Science*, **15**, 1308781.

Vayghan H S, Nawrocki W J, Schiphorst C, Tolleter D, Hu C, Douet V, Glauser G, Finazzi G, Croce R, Wientjes E, Longoni F. 2022. Photosynthetic light harvesting and thylakoid organization in a CRISPR/Cas9 *Arabidopsis thaliana* LHCB1 knockout mutant. *Frontiers in Plant Science*, **13**, 833032.

Wan S, Wu J, Zhang Z, Sun X, Lv Y, Gao C, Ning Y, Ma J, Guo Y, Zhang Q, Zheng X, Zhang C, Ma Z, Lu T. 2009. Activation tagging, an efficient tool for functional analysis of the rice genome. *Plant Molecular Biology*, **69**, 69–80.

Wang X, Pan C, Long J, Bai S, Yao M, Chen J, Sun G, Fan Y, Wang Z, Liu F, Liu C, Li Q. 2022. Genome-wide identification of the jumonji C domain- containing histone demethylase gene family in wheat and their expression analysis under drought stress. *Frontiers in Plant Science*, **13**, 987257.

Wang Y, Perez-Sancho J, Platre M P, Callebaut B, Smokvarska M, Ferrer K, Luo Y, Nolan T M, Sato T, Busch W, Benfey P N, Kvasnica M, Winne J M, Bayer E M, Vukašinović N, Russinova E. 2023. Plasmodesmata mediate cell-to-cell transport of brassinosteroid hormones. *Nature Chemical Biology*, **19**, 1331–1341.

Wei T, Zhang L, Zhu R, Jiang X, Yue C, Su Y, Ren H, Wang M. 2021. A gain-of-function mutant of IAA7 inhibits stem elongation by transcriptional repression of *EXPA5* genes in *Brassica napus*. *International Journal of Molecular Sciences*, **22**, 9018.

Wei Z, Li J. 2020. Regulation of brassinosteroid homeostasis in higher plants. *Frontiers in Plant Science*, **11**, 583622.

Wolf S. 2022. Cell wall signaling in plant development and defense. *Annual Review of Plant Biology*, **73**, 323–353.

Wu M, Ren Y, Cai M, Wang Y, Zhu S, Zhu J, Hao Y, Teng X, Zhu X, Jing R, Zhang H, Zhong M, Wang Y, Lei C, Zhang X, Guo X, Cheng Z, Lin Q, Wang J, Jiang L, *et al.* 2019. Rice FLOURY ENDOSPERM10 encodes a pentatricopeptide repeat protein that is essential for the *trans*-splicing of mitochondrial *nad1* intron 1 and endosperm development. *New Phytologist*, **223**, 736–750.

Yang M, He J, Wan S, Li W, Chen W, Wang Y, Jiang X, Cheng P, Chu P, Shen W, Guan R. 2021. Fine mapping of the *BnaC04.BIL1* gene controlling plant height in *Brassica napus* L. *BMC Plant Biology*, **21**, 359.

Yang Z, Wang S, Wei L, Huang Y, Liu D, Jia Y, Luo C, Lin Y, Liang C, Hu Y, Dai C, Guo L, Zhou Y, Yang Q Y. 2023. BnIR: A multi-omics database with various tools for *Brassica napus* research and breeding. *Molecular Plant*, **16**, 775–789.

Zebosi B, Vollbrecht E, Best N B. 2024. Brassinosteroid biosynthesis and signaling: conserved and diversified functions of core genes across multiple plant species. *Plant Communications*, **5**, 100982.

Zhan H, Lu M, Luo Q, Tan F, Zhao Z, Liu M, He Y. 2022. *OsCPD1* and *OsCPD2* are functional brassinosteroid biosynthesis genes in rice. *Plant Science*, **325**, 111482.

Zhang H, Zhao D, Tang Z, Zhang Y, Zhang K, Dong J, Wang F. 2022. Exogenous brassinosteroids promotes root growth, enhances stress tolerance, and increases yield in maize. *Plant Signaling & Behavior*, **17**, 2095139.

Zhang X, Lin R. 2017. Light signaling differentially regulates the expression of group IV of the B-box zinc finger family. *Plant Signaling & Behavior*, **12**, e1365213.

Zhao B, Li H, Li J, Wang B, Dai C, Wang J, Liu K. 2017. *Brassica napus DS-3*, encoding a DELLA protein, negatively regulates stem elongation through gibberellin signaling pathway. *Theoretical and Applied Genetics*, **130**, 727–741.

Zhao B, Li J. 2012. Regulation of brassinosteroid biosynthesis and inactivation. *Journal of Integrative Plant Biology*, **54**, 746–759.

Zhao C, Yang L, Tang M, Liu L, Huang J, Tong C, Xiang Y, Liu S, Cheng X, Xie M. 2022. Genome-wide association study reveals a *GLYCOGEN SYNTHASE KINASE 3* gene regulating plant height in *Brassica napus*. *Frontiers in Plant Science*, **13**, 1061196.

Zheng M, Terzaghi W, Wang H, Hua W. 2022. Integrated strategies for increasing rapeseed yield. *Trends in Plant Science*, **27**, 742–745.

Zheng M, Zhang L, Tang M, Liu J, Liu H, Yang H, Fan S, Terzaghi W, Wang H, Hua W. 2020. Knockout of two *BnaMAX1* homologs by CRISPR/Cas9-targeted mutagenesis improves plant architecture and increases yield in rapeseed (*Brassica napus* L.). *Plant Biotechnology Journal*, **18**, 644–654.

Zhiponova M K, Vanhoutte I, Boudolf V, Betti C, Dhondt S, Coppens F, Mylle E, Maes S, González-García M P, Caño-Delgado A I, Inzé D, Beemster G T S, De Veylder L, Russinova E. 2013. Brassinosteroid production and signaling differentially control cell division and expansion in the leaf. *New Phytologist*, **197**, 490–502.

Zhou X, Zhang H, Wang P, Liu Y, Zhang X, Song Y, Wang Z, Ali A, Wan L, Yang G, Hong D. 2022. *BnaC7.ROT3*, the causal gene of cqSL-C7, mediates silique length by affecting cell elongation in *Brassica napus*. *Journal of Experimental Botany*, **73**, 154–167.

Zhu L, Wang H, Zhu J, Wang X, Jiang B, Hou L, Xiao G. 2023. A conserved brassinosteroid-mediated BES1-CERP-EXPA3 signaling cascade controls plant cell elongation. *Cell Reports*, **42**, 112301.

Executive Editor-in-Chief Xueyong Zhang
Managing Editor Ning Wang